Acta Materialia 228 (2022) 117780

Contents lists available at ScienceDirect

Acta Materialia

journal homepage: www.elsevier.com/locate/actamat

Full length article

Analysis of temperature gradient zone melting and the thermal migration of liquid particles through a solid

Swanand Pawar, Kerry P. Wang, Andrew Yeckel, Jeffrey J. Derby*

Department of Chemical Engineering and Materials Science, University of Minnesota, Minneapolis, MN 55455, USA

ARTICLE INFO

Article history:
Received 8 November 2021
Revised 28 January 2022
Accepted 18 February 2022
Available online 20 February 2022

Keywords:
Droplets
Gradient
Particle
Solid/liquid interface
TGZM

ABSTRACT

Analytical solutions are derived to describe the migration of a liquid particle or droplet, enriched in one component, through a solid under a thermal gradient, a behavior also known as temperature gradient zone melting or TGZM. Such a particle migrates in the direction of increasing temperature and is driven by different temperatures and equilibrium compositions that produce dissolution of the solid matrix at the leading end, regrowth at the trailing end, and diffusion of the excess component across the droplet. While simple, linear concentration and temperature profiles arise within the liquid particle during migration, both droplet velocity and size exhibit nonlinear growth with time. Conditions for the validity of the analytical TGZM solutions are identified, and suggestions are put forth for experimental application and further improvements.

1. Introduction

Liquid or vapor particles, enriched in a component, can be induced to migrate through a solid under a temperature gradient. Such particles are commonly found in many natural systems and in synthetically manufactured solids and crystals. By the actions of thermal and molecular diffusion, dissolution or sublimation at the hotter interface, and freezing or condensation at the cooler interface, such particles migrate toward the direction of higher temperature. For liquid zones or droplets in manufactured solids, this phenomenon has been commonly referred to as temperature gradient zone melting, or TGZM [1,2].

A number of scientific and engineering disciplines would benefit from a more quantitative understanding of this migration process. For example, particle migration plays an important role in safe nuclear energy production—bubbles that cause swelling in nuclear fuel elements [3–5] and brine particles in salt mines used for nuclear waste storage are observed to migrate over time [6]. In another important area, understanding of paleoclimate is derived from chemical analysis of entrained particles in ice core samples, but migration of brine particles may shift paleoclimate signals by thousands of years [7]. Thermal migration influences interdendritic pools and secondary dendritic arms during the directional solidification of alloys [8–12]. Finally, devices fabricated from compound semiconductors are often degraded by the presence of second-phase particles, such as Te-rich particles in bulk crystals of CdTe and CdZnTe, which are important materials for high-performance, room-temperature x-ray and gamma-ray detectors [13–16]. These second-phase particles can be induced to melt and migrate under the application of suitably high temperatures and spatial thermal gradients [17–27], potentially improving material quality and device performance.

In this paper, we mathematically model the thermal migration of a second-phase, liquid particle in a solid and derive an analytical solution from governing equations of heat and mass transfer, coupled with thermodynamics. We discuss the behavior of the system predicted by the model and the limits of applicability of this approximate solution. This derivation and subsequent discussion offer significant insight into the mechanisms that drive particle migration.

2. Background and prior work

2.1. Historical and physical context

In 1926, Whitman [28] first described a mechanism by which brine inclusions migrate in sea ice under natural temperature gradients, informed from the correspondence of Canadian Arctic explorer Dr. Vilhjalmur Stefansson, who, five years earlier, wrote [29]:

> Pieces of sea-water ice, only a few days old, are too salty for cooking or drinking purposes... On the other hand, the saltiness of ice that has floated in the ocean during a warm season has decreased to such an extent that it is potable.

* Corresponding author.
E-mail address: derby@umn.edu (J.J. Derby).

https://doi.org/10.1016/j.actamat.2022.117780
1359-6454/

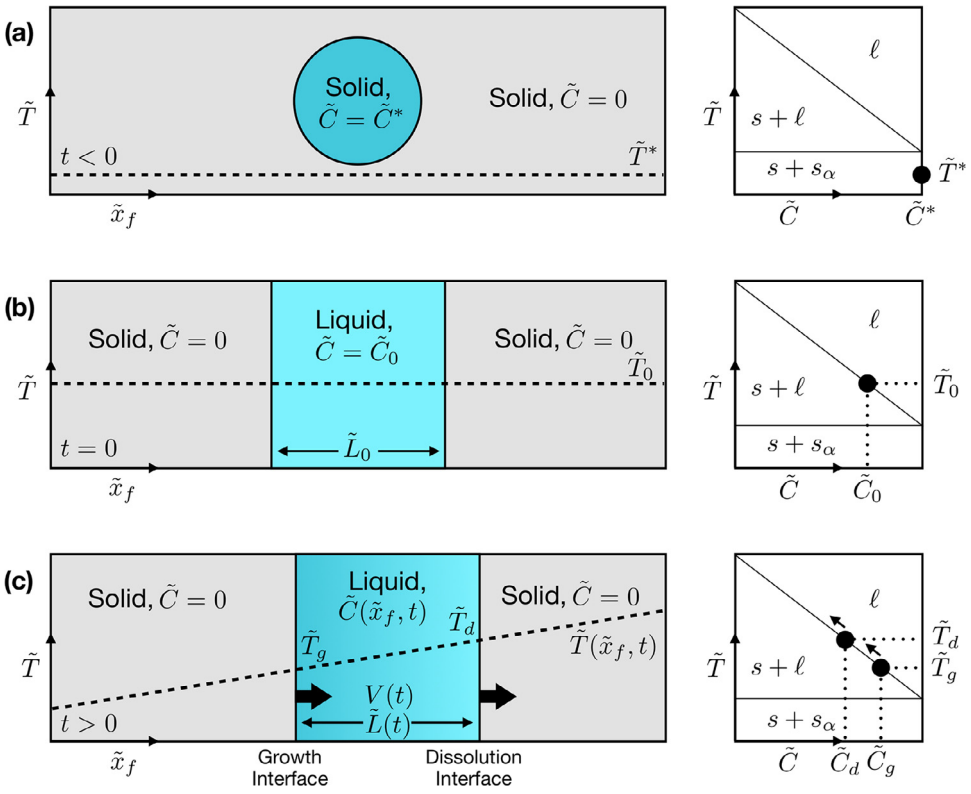

Fig. 1. Depictions of our particle migration model for TGZM. Images on the left show the physical state of the particle within the matrix, and diagrams on the right indicate system states on the equilibrium phase diagram.

Brine inclusions are captured during the freezing of seawater. With a lower freezing point, these brine particles remain liquid while the surrounding ice crystal of relatively pure water remains solid. Whitman hypothesized that a difference in temperature between the atmosphere and surrounding seawater sets up a thermal gradient that drives migration, eventually causing the brine particle to expel itself from the sea ice. Due to the dependence of the thermodynamic melting temperature on composition, the warmer side of a brine droplet melts the surrounding ice, while the cold side refreezes it. Whitman surmised that, "A continuation of this process would result in steady diffusion of the brine droplet out to the warmer end and would eventually eliminate it from the ice."

Let us more closely analyze the physical mechanisms that are occurring during the thermal migration of a liquid inclusion, hereafter referred to simply as a particle or droplet. These particles consist of a different thermodynamic phase than the surrounding solid, hence the term second-phase particles, and they are present in the solid due to two possible mechanisms. First, they may be precipitates that have nucleated and grown when the solid becomes supersaturated with one component, typically due to retrograde solubility during the cooling from a high synthesis temperature to room temperature, such as during crystal growth or solidification processes. Second, they may have formed via inclusion processes, such as droplet capture, driven by unstable solidification conditions, typically due to constitutional supercooling [30–34]. In either case, these particles are enriched in a chemical species or component, as compared to the composition of the surrounding solid material that is nearly pure or in stoichiometric proportion. The enriched or excess component has been variously termed dopant, solute, solvent, brine, or salt, depending upon the circumstances involved with the formation of the underlying solid.

Consider a material that is represented by the idealized phase diagram, shown to the right in Fig. 1, where the equilibrium thermodynamic phase at constant pressure is indicated as a function of temperature, $\tilde{T}$, and composition in excess of the pure or stoichiometric solid, $\tilde{C}$. To simplify our discussion, we consider that the solidus curve is vertical, indicating that a pure substance solidifies from all liquid compositions, with a distribution coefficient of $K = 0$ for the solute. While a perfectly vertical solidus is not entirely realistic, it is nevertheless a very reasonable approximation to the very small distribution coefficient, typically $K \ll 1$, for systems that exhibit second-phase particles.

Fig. 1 (a) depicts the system at a low temperature $\tilde{T}^*$, where two solid phases are in equilibrium, comprising the stoichiometric solid, s, and a solute-rich phase, s_α, of concentration $\tilde{C}^*$, as indicated by the point shown on the phase diagram to the right. The second-phase particle is represented schematically in the left image as a sphere embedded within the surrounding matrix. At an elevated temperature $\tilde{T}_0$ in an isothermal setting, the particle and some of the surrounding pure solid will melt and establish an equilibrium concentration $\tilde{C}_0$, as indicated in Fig. 1(b). We denote this time as $t = 0$, when the second-phase particle is a liquid but stationary, since it is in equilibrium with the solid matrix. We also schematically represent our forthcoming mathematical analysis by converting the initially three-dimensional solid particle into a one-dimensional liquid zone of length $\tilde{L}_0$.

Upon the instantaneous application of a temperature gradient at $t > 0$, the liquid particle is no longer in equilibrium with the surrounding solid, and several simultaneous and coupled processes are initiated; see Fig. 1(c). The liquid at the cooler side of the particle is now undercooled and is too dilute to be in equilibrium with its thermal environment. Thus, the cooler interface moves to the right, growing new solid. Conversely, the liquid at the warmer side of the particle is now superheated and is too concentrated to be in equilibrium with its thermal environment. The warmer interface dissolves, with movement of the interface to the right. The net effect of growth at the cooler interface and dissolution at the warmer interface is the migration of the liquid particle in the up-

hill direction of the temperature gradient, with the droplet center moving at a velocity V.

This growth and dissolution, first described by Whitman [28], occurs so that the solid-liquid interfaces can achieve a state more closely resembling equilibrium, with the growth and dissolution interfaces at temperatures $\tilde{T}_g$ and $\tilde{T}_d$, respectively, and the composition of the liquid adjacent to these interfaces prescribed by the liquidus curve at $\tilde{C}_g$ and $\tilde{C}_d$; see Fig. 1(c). However, growth and dissolution continually shift the state away from equilibria at the interfaces. Specifically, the formation of pure solid at the growth interface rejects solute into the liquid, and the melting of pure solid at the dissolution interface dilutes it. This produces a concentration gradient that leads to solute diffusion across the particle, from the growth to the dissolution interface.

Simultaneously, the particle is moving up the temperature gradient, as indicated by the arrows on the phase diagram shown in Fig. 1(c). Since the interfaces are always seeking a near-equilibrium state, the liquid solute concentrations at both interfaces must *decrease*, per the negative slope of the liquidus, as the particle migrates. For a system with a vertical solidus curve, the composition of the solid on both sides of the particle is unchanged, thus the total amount of solute in the particle must remain constant, even though the particle is moving up the liquidus curve and its average concentration level is decreasing. Conservation of mass thus requires that the particle must *increase* in size during migration. Thus, particle migration via TGZM is an inherently transient phenomenon, and there is no true steady state describing particle migration.

2.2. Experimental studies

After the pioneering work on brine inclusion migration by Whitman [28], the next advance in the understanding of the migration of liquid zones in solids occurred decades later, in the field of electronic materials. In 1954, Pfann [2] filed a patent on an industrial semiconductor doping process, whereby a crystal containing a zone of high dopant concentration is annealed under a temperature gradient, which subsequently moves the zone and leaves behind a re-grown, doped solid. He later more generally described how, by the same physical mechanisms as brine expulsion in ice, the liquid zone migrates in the direction of the temperature gradient. He furthermore suggested several possible uses of this effect, such as fabricating semiconductor devices, growing single crystals, joining, boring fine holes in solids, measuring diffusivities in liquids, small scale alloying, and purification [1]. Pfann coined the term *temperature gradient zone melting* or TGZM to describe this process, which has subsequently been widely adopted.

Pfann's patent [2] discussed operating principals and furnace design schematics that would perform this industrial process for semiconductors such as germanium and silicon. Wernick [35] performed experiments on molten aluminum and gold wire migration in silicon and germanium solids and reported that migration velocity was dependent on wire thickness and material orientation, implying that the kinetics of melting and solidification on certain crystallographic faces were playing a role. However, Mlavsky and Weinstein found no such orientation-dependency in studies of gallium zones in gallium arsenide [36].

Kingery and Goodnow [37] performed experiments on NaCl and KCl brine particles undergoing thermal migration in ice. They measured particle velocities and provided analytical expressions for particle migration behavior through the use of diffusion equations. Wilcox [38] provided an overview of gradient techniques to remove inclusions from crystals, with an extensive summary of prior experimental observations of the kinetics of the thermal migration of liquid droplets. Anthony and Cline [39–41] performed experiments in a number of different system and devised mathematical models to describe the effects of interfacial kinetics on migrating particles. Jones performed experiments to measure kinetic coefficients for ice-brine interfaces from the shapes of migrating droplets in thermal gradients [42–44].

In metallurgical applications, Allen and Hunt [8] were the first to identify the influence of TGZM on the development of secondary arm spacing on dendrites during directional solidification. Later, Thi et al. [9] confirmed TGZM effects occurred during the solidification of aluminum-based alloys using in situ, synchrotron x-radiography. Rettenmayr [10] discussed the importance of TGZM during solidification in an overview of melting and remelting phenomena.

TGZM has been studied as a means to ameliorate Te-rich, second-phase particles that are prevalent in bulk, single crystals of the II-VI semiconductors CdTe and CdZnTe, grown for infrared and gamma radiation detector applications [15,16]. Early observations indicated that the Te-rich inclusions migrated under the thermal gradients during crystal growth of these compounds [13–16]. Post-growth annealing of CdZnTe under temperature gradients has been investigated to use thermomigration to sweep these second-phase particles from bulk samples and thereby improve substrate quality [17–27].

2.3. Modeling of TGZM

The first theoretical treatment of TGZM was put forth by Tiller [45] in 1963. In Tiller's analysis, pseudo-steady thermal fields are determined by the Laplace heat diffusion equation, and interface velocities are determined by kinetic models of melting and freezing under the surrounding thermal profile. Tiller's solutions presented several scenarios to explain particle migration velocities, but his analysis perhaps unduly emphasized the importance of interfacial kinetics. In their analysis of TGZM effects on secondary dendritic arm spacing, Allen and Hunt [8] built upon prior work [39,45,46] to derive an expression for the velocity of a migrating liquid zone in a stationary temperature gradient.

Toward explaining the migration of brine pockets in ice, Hoekstra et al. [47] derived expressions for migration velocity similar to those derived by Kingery and Goodnow [37] and argued that the qualitative agreement between their derived model and experimental data suggested that kinetics of melting and freezing were likely not the dominant rate-controlling mechanism. Seidensticker [48] improved on this model by accounting for changes in solute diffusivity as a function of temperature, leading to better agreement with the experimental results of Hoekstra et al. [47]. Shreve [49] derived expressions for migration velocity of particles of various geometries such as spheres, ellipsoids, and cylinders, and accounted for orientation effects relative to direction of the thermal gradient.

The long history of analyses of TGZM and thermal migration speak to the particular challenges of posing and solving this problem. While Tiller [45] emphasized kinetic phenomena at the growth and dissolution interfaces, analytical solutions for these cases proved to be too unwieldy to employ in practice and empirical observations generally did not support the postulated importance of interface kinetics. However, in the absence of kinetic factors, Tiller derived the following expression for particle velocity,

$$V = \frac{G\mathcal{D}}{(1-K)m\tilde{C}}, \tag{1}$$

where G is the imposed thermal gradient through the sample, $\mathcal{D}$ is the liquid-phase diffusivity of the excess component, K is the equilibrium distribution coefficient, m is the slope of the liquids curve, and $\tilde{C}$ is the concentration of the excess component in the particle. Very similar expressions were also derived by Hoekstra

et al. [47], Seidensticker [48], Wilcox [38], Cline and Anthony [41], and Allen and Hunt [8]. These results identify the essence of the driving forces for TGZM as the temperature gradient balanced by solute diffusion across the particle, which is driven by the different, equilibrium solute concentrations at the growth and dissolution interfaces. However, all of these models invoked steady-state arguments that were not reconciled with the inherently transient behavior of particle migration, as discussed in the previous section.

More recently, Pan et al. [11], building upon the analysis of Allen and Hunt [8], realized that the particle position is a function of time and that its composition is therefore also a function time. Starting with Eq. (1), Pan et al. were able to derive an ordinary differential equation defining the particle position and solve it analytically. They furthermore demonstrated good agreement between their analytical result and a phase-field numerical solution for a model alloy solidification problem [12]. While this analytical solution represented a significant advance in the quantitative understanding of TGZM, it did not explicitly provide solutions for the changing length of the particle nor the form of the temperature and concentration profiles within the particle as time evolves. Finally, there is little discussion in [11] of their derivations or of the underlying approximations employed by Allen and Hunt [8], which was the starting point for their analysis.

In the following discussion, we seek to more fully address the formulation, solution, and limitations of an analytical solution describing liquid particle migration under an imposed thermal gradient in TGZM.

3. Model formulation and solution

3.1. Scaling and initial assumptions

Following our above discussion associated with Fig. 1, we employ a one-dimensional representation of the liquid particle or droplet containing an excess of one component migrating through a binary solid. The droplet is assumed to be a liquid initially in thermodynamic equilibrium with the surrounding, constant-composition solid. Immediately after time zero, a linear temperature profile is applied across the system, and the particle begins migrating. We presume that there is no density change between solid and liquid, so that there is no bulk flow within the moving particle. We assume that the solid is everywhere of stoichiometric composition and that there is no redistribution of solute within the solid.

Within the context of this one-dimensional particle, there are two interfaces, one at which growth occurs and the other at which there is dissolution. We neglect any kinetic effects associated with growth or dissolution and assume that both interfaces are under local thermodynamic equilibrium. Finally, we cannot represent the shape of this one-dimensional particle, only its evolving length. We therefore neglect the effect of local interfacial curvature on melting point, as would be dictated by the Gibbs–Thomson effect for a particle with curved interfaces. This model limitation is further discussed in the conclusions section.

We specifically consider the case of a binary system, under constant pressure, governed by a simple phase diagram that exhibits a linear liquidus curve and a vertical solidus curve, as was depicted schematically in Fig. 1. Such phase behavior is meant to capture the essence of binary systems, in which the excess component serves as a solvent in the liquid phase but is not present beyond stoichiometric amounts in the solid. We choose to represent composition in terms of the mole fraction in excess of the binary solid composition. This excess mole fraction, $\tilde{C}$, is given by $\tilde{C} = \tilde{C}_\ell - \tilde{C}_s$, where $\tilde{C}_\ell$ is the mole fraction of excess component in the liquid and $\tilde{C}_s$ is the mole fraction of that component in the stoichiometric solid. This definition provides a particularly simple mathematical representation of the liquidus curve of the phase diagram,

$$\tilde{T}(\tilde{C}) = T_{mp} - m\tilde{C}, \tag{2}$$

where $\tilde{T}(\tilde{C})$ is the composition-dependent melting temperature, T_{mp} is the melting point of the stoichiometric solid, and m is the absolute value of the slope of the liquidus line.

We next define a coordinate system, $\tilde{x}$, in which the center of the particle is immobilized and mapped to $\tilde{x} = 0$. With respect to the fixed, laboratory frame of reference,

$$\tilde{x} = \tilde{x}_f + \int_0^t V(s)\, ds, \tag{3}$$

where $\tilde{x}_f$ denotes the laboratory frame, $V(t)$ is the instantaneous velocity of the center of the particle, and t is time. In this moving coordinate, the underlying material is moving with a speed $V(t)$ in the negative direction.

We define a dimensionless coordinate as $x \equiv \tilde{x}/\tilde{L}_0$, where $\tilde{L}_0$ is the initial length of the one-dimensional particle. The size of the particle is expected to change in time and is made dimensionless as, $L(t) \equiv \tilde{L}(t)/\tilde{L}_0$, with its endpoints defined by a dissolution interface at $x = L/2$ and a growth interface at $x = -L/2$. This coordinate transformation and the resulting thermal and concentration profiles across the droplet are schematically represented in Fig. 2.

Seeking to simplify the problem using scaling, we define a characteristic time scale associated with the diffusion of the excess component across the particle as $\tau_{\mathcal{D}} \equiv \tilde{L}_0^2/\mathcal{D}$, where $\mathcal{D}$ is the liquid-phase diffusion coefficient of the excess component, and we define dimensionless time as $\tau \equiv t/\tau_{\mathcal{D}}$. We invoke a quasi-steady-state (QSS) approximation that considers both the particle velocity and length, $V(t)$ and $L(t)$, to vary on a much longer time scale than $\tau_{\mathcal{D}}$. Using this approach, the temperature and composition are presumed to exhibit quasi-steady-state profiles through the particle, represented by functions of x only. Justification for the QSS assumption will be further discussed following the solution derivation in Section 4.2.

Next, we choose to nondimensionalize the QSS concentration as,

$$C(x) \equiv \frac{\tilde{C}}{\tilde{C}_0}, \tag{4}$$

where $\tilde{C}_0$ is the mole fraction of excess component in the initial particle. This simple scaling sets the maximum dimensionless composition as unity.

We define a nondimensional QSS temperature as,

$$T(x) \equiv \frac{\tilde{T} - T_{mp}}{\kappa G \tilde{L}_0}, \tag{5}$$

where the reference temperature, T_{mp}, is the melting point of the pure or stoichiometric solid and the characteristic temperature scale is chosen as the temperature difference across the droplet, which is given by the product of $\kappa \equiv k_s/k_\ell$, the ratio of thermal conductivities between the solid and liquid, G, the temperature gradient applied across the solid, and $\tilde{L}_0$, the initial length of the droplet. This definition is somewhat unconventional, since the resulting dimensionless temperature is negative and its magnitude depends upon the arbitrary parameter G. However, this choice allows a particularly simple dimensionless representation of the equlibrium liquidus curve, Eq. (2), as,

$$T_{eq}(C) = -\varepsilon^{-1} C, \tag{6}$$

and also reveals a significant dimensionless group, given by,

$$\varepsilon \equiv \frac{\kappa G \tilde{L}_0}{m\tilde{C}_0}. \tag{7}$$

This combination of physical properties and process parameters represents a ratio of the temperature change across the droplet

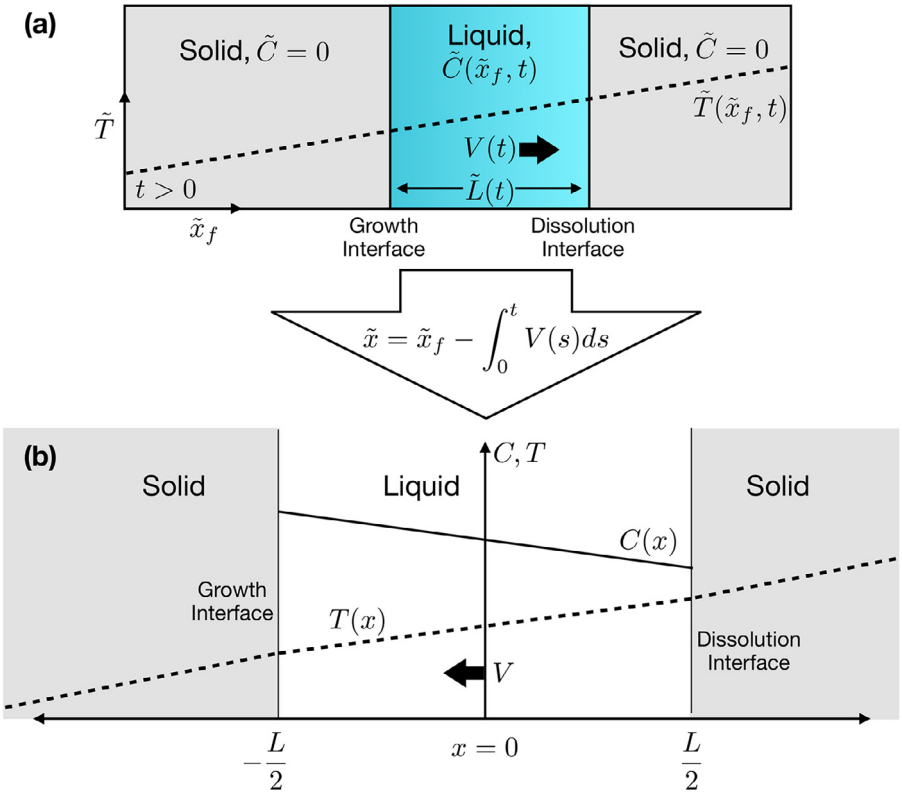

Fig. 2. The migrating liquid particle depicted in (a) is mapped into (b), a one-dimensional, moving coordinate system in which the dissolution and growth interfaces are located at $x=\pm L/2$, respectively. In the moving coordinate system, there is an apparent velocity directed in the negative direction, and application of the quasi-steady-state (QSS) approximation makes the concentration and temperature profiles through the liquid to be functions of only x.

scaled by a measure of the compositional effect on the equilibrium melting temperature, which are the two driving forces for particle migration. Henceforth, we shall refer to ε as the dimensionless migration parameter.

3.2. QSS concentration field

We presume that diffusion of the excess component through the surrounding solid matrix is negligible, so we need only consider the concentration profile within the liquid particle. Using the scalings defined above, we write a one-dimensional transport equation for the excess component within the particle, for $-L/2 \le x \le L/2$, as,

$$\frac{\partial C}{\partial \tau} - Pe\frac{\partial C}{\partial x} = \frac{\partial^2 C}{\partial x^2}, \tag{8}$$

where the dimensionless Peclet number is defined as,

$$Pe \equiv V\tilde{L}_0/\mathcal{D}. \tag{9}$$

Note that in our coordinate frame attached to the moving particle, there is a flow of liquid at velocity V in the negative x-direction, thereby giving rise to the negative sign preceding the second term of the left-hand-side of the above equation, which represents the effects of convection.

The Peclet number arises naturally in the above dimensionless equation to multiply the convective transport term. However, it also takes on a special meaning in this problem, since it is defined using the time-dependent velocity, $V(\tau)$. Thus, the Peclet number also is the dimensionless representation of the particle velocity in this problem.

We first invoke the quasi-steady-state (QSS) assumption to set $\partial C/\partial\tau = 0$ and rearrange the governing equation to yield,

$$\frac{\partial^2 C}{\partial x^2} + Pe\frac{\partial C}{\partial x} = 0. \tag{10}$$

Next, we assert that $Pe \ll 1$ in the TGZM problem, so that the second term is much smaller than the first term and can can be neglected, giving us,

$$\frac{\partial^2 C}{\partial x^2} = 0. \tag{11}$$

The concentration profile through the particle then has the very simple form of,

$$C(x) = Ax + B, \tag{12}$$

where A and B are constants to be determined.

We follow with dimensionless conditions that balance species fluxes across each interface. These take the following forms at the growth interface, located at $x=-L/2$,

$$\left.\frac{dC}{dx}\right|_{x=-L/2} + C(-L/2)\left[Pe - \frac{1}{2}\frac{dL}{d\tau}\right] = 0, \tag{13}$$

and along the dissolution interface, at $x=L/2$,

$$\left.\frac{dC}{dx}\right|_{x=L/2} + C(L/2)\left[Pe + \frac{1}{2}\frac{dL}{d\tau}\right] = 0. \tag{14}$$

Note that the second term of these equations represents the convective flux of species across each interface, including a velocity for flow in the liquid caused by the motion of the particle, given by Pe, and an interface velocity in the coordinate frame that distributes one half of the droplet length expansion, $dL/d\tau$, to each interface. We also note that these conditions reflect our simplified phase diagram with a distribution coefficient of $K=0$.

We again assert the quasi-steady-state assumption to neglect the droplet expansion terms involving $dL/d\tau$ and apply the above conditions. We find that only one of the constants in the linear concentration profile of Eq. (12) is determined by these conditions,

since both specify fluxes, and we calculate the following consistent result, valid for $Pe \ll 1$,

$$A = -PeB. \tag{15}$$

To determine the value of B, we argue that the total amount of excess component in the liquid zone must remain constant, since, consistent with our assumption of $K = 0$, none enters or leaves the zone at either interface. Hence, we apply an integral mass balance, given in dimensionless terms as,

$$\int_{-L/2}^{L/2} C(x)\, dx = 1, \tag{16}$$

where the total excess solute in the particle is $\tilde{C}_0\tilde{L}_0$ in dimensional terms and unity in dimensionless terms. Evaluating this intergal using in Eq. (12) with the previously determined value for A gives

$$B = 1/L, \tag{17}$$

thereby providing the solution for the concentration profile in the droplet as,

$$C(x) = \frac{1}{L}(1 - Pe\, x). \tag{18}$$

Note that the negative slope of this profile shows that the excess component diffuses in the positive direction. Excess solute is rejected at the growth interface and diffuses across the particle to the lower-concentration dissolution interface. The value of concentration at the center of the droplet, at $x = 0$, is given by $1/L$, which is also the average dimensionless concentration in the particle. Thus, the average droplet concentration decreases as the length of the particle increases with time, which is consistent with the arguments put forth describing TGZM with Fig. 1.

3.3. QSS temperature field

In nondimensional terms, the energy conservation equation for one-dimensional heat transfer within the droplet is given as,

$$Le^{-1}\left(\frac{\partial T}{\partial \tau} - Pe\frac{\partial T}{\partial x}\right) = \frac{\partial^2 T}{\partial x^2}, \tag{19}$$

where the dimensionless Lewis number is defined by $Le \equiv \alpha_\ell/\mathcal{D}$, where $\alpha_\ell \equiv k_\ell/(\rho_\ell C_p)$ is the thermal diffusivity of the liquid, with k_ℓ, ρ_ℓ, and C_p, representing density, heat capacity, and thermal conductivity, respectively. Note in the above equation that the product of the inverse Lewis number and the Peclet number could also be represented as $Le^{-1}Pe \equiv Pe_h = VL_0/\alpha_\ell$, where Pe_h is a dimensionless Peclet number for heat transfer. Invoking the QSS assumption, we set the time-derivative in the above equation to zero to obtain,

$$-Le^{-1}Pe\frac{\partial T}{\partial x} = \frac{\partial^2 T}{\partial x^2}. \tag{20}$$

The Lewis number, representing the ratio of thermal diffusivity to mass diffusivity, is typically very large for liquids so that $Le^{-1} \ll 1$. Thus, compared to the order unity term on the right-hand-side of the equation, we ignore the convective term multiplied by $Le^{-1}Pe$ and arrive at the heat conduction equation,

$$\frac{\partial^2 T}{\partial x^2} = 0. \tag{21}$$

Of course, the temperature profile is that satisfies this governing equation is simply,

$$T(x) = Dx + E, \tag{22}$$

where D and E are to be determined.

The temperature field must be continuous between liquid and solid and heat must be conserved at both the growth and dissolution interfaces. The following dimensionless conditions enforce a heat balance over the growth interface at $x = -L/2$,

$$\left[\kappa\left.\frac{dT}{dx}\right|_s - \left.\frac{dT}{dx}\right|_\ell\right]_{x=-L/2} = SfLe^{-1}\left[Pe - \frac{1}{2}\frac{dL}{d\tau}\right], \tag{23}$$

and over the dissolution interface at $x = L/2$,

$$\left[\kappa\left.\frac{dT}{dx}\right|_s - \left.\frac{dT}{dx}\right|_\ell\right]_{x=L/2} = -SfLe^{-1}\left[Pe + \frac{1}{2}\frac{dL}{d\tau}\right], \tag{24}$$

where $\kappa \equiv k_s/k_\ell$ is the ratio of thermal conductivities between the solid and liquid and the dimensionless Stefan number is defined here as,

$$Sf \equiv \frac{-\Delta H_f}{C_p \kappa G \tilde{L}_0}, \tag{25}$$

with ΔH_f denoting the latent heat of solidification, which by convention is negative, making the Stefan number positive. Note that, similar to the species flux conditions of the previous section, eqs. (13) and (14), terms accounting for the motion of the interfaces by droplet expansion, $dL/d\tau$, are included. In addition, latent heat of phase change is released upon the formation of solid from liquid but absorbed when a solid melts or dissolves into a liquid. Thus, the signs of the right-hand-side of the above heat flux balances are reversed at the growth and dissolution interfaces.

We invoke the QSS assumption to set $dL/d\tau = 0$ and argue that the remaining terms on the right-hand-side can be disregarded compared to the order-unity terms on the left-hand-side. This will be true when $SfLe^{-1}Pe \ll 1$, indicating that latent heat is unimportant. Thus, we assert that both of the interface heat flux conditions reduce to,

$$\left.\frac{dT}{dx}\right|_\ell = \kappa\left.\frac{dT}{dx}\right|_s = 1, \tag{26}$$

where the value of unity arises from the definition of our dimensionless variables along with the realization that, when latent heat effects are negligible, the dimensional thermal gradient is constant everywhere in the solid and equal to the imposed value of G. Thus, for Eq. (22), we evaluate the constant $D = 1$.

We follow this to evaluate E by applying equilibrium conditions at either solid-liquid interface,

$$T(\pm L/2) = T_{eq}(C(\pm L/2)). \tag{27}$$

Choosing the dissolution interface at $x = L/2$, we evaluate the left-hand-side of the above equation using the solution for the temperature field across the particle, Eq. (22), followed by evaluation of the right-hand-side via the liquidus definition of Eq. (6), to arrive at

$$E = -\frac{1}{\varepsilon L} + \frac{Pe}{2\varepsilon} - \frac{L}{2}. \tag{28}$$

We may neglect the second term on the right-hand-side of the above expression via our assertion that $Pe \ll 1$, and the third term may be ignored if

$$\varepsilon \ll 2/L^2, \tag{29}$$

a condition that will be demonstrated to hold in Section 4.2.2. The remaining, dominant term of Eq. (28) leads to $E = -1/\varepsilon L$.

After the determinations of these constants, we finally obtain the temperature profile through the droplet as,

$$T(x) = x - \frac{1}{\varepsilon L}. \tag{30}$$

3.4. Transient evolution

The above analysis applied the quasi-steady-state assumption to claim that both $V(\tau)$ and $L(\tau)$ change on a much slower time scale than the temperature and concentration profiles over the particle. Let us now explicitly examine the transient nature of the velocity and length of the migrating particle.

We first re-consider the conditions enforcing local thermodynamic equilibrium at both solid-liquid interfaces, namely Eq. (27), and use the temperature profile, Eq. (30), to evaluate the left-hand side, along with the liquidus curve, Eq. (6), yielding conditions at the growth and dissolution interfaces of,

$$-\frac{L}{2}-\frac{1}{\varepsilon L}=-\frac{1}{\varepsilon L}(1+Pe\frac{L}{2}), \tag{31}$$

$$\frac{L}{2}-\frac{1}{\varepsilon L}=-\frac{1}{\varepsilon L}(1-Pe\frac{L}{2}). \tag{32}$$

Subtracting one equation from the other and rearranging yields a very useful result, namely,

$$Pe=\varepsilon L, \tag{33}$$

which is a dimensionless equation for the instantaneous particle velocity, since $V(\tau)$ is embedded within Pe. This expression shows that the particle velocity increases as its length, $L(\tau)$, increases during migration. We also note from this expression that the dimensionless migration parameter ε can also be interpreted as a dimensionless initial particle velocity, since $L(0)=1$.

To evaluate the velocity as a function of time, we need an expression for the time-dependent length of the particle. For this, we return to the solute balances over each interface. In contrast to their use in arriving at the concentration profile, the terms involving $dL/d\tau$ are not discarded, and eqs. (13) and (14) are subtracted. Evaluating interfacial concentrations using the concentration profile, Eq. (18), we get,

$$\frac{dL}{d\tau}=Pe^2L \tag{34}$$

rearranging and substituting for $Pe=\varepsilon L$ from Eq. (33) above yields,

$$\frac{dL}{d\tau}=\varepsilon^2L^3. \tag{35}$$

With the initial condition that $L(0)=1$, the above equation is solved analytically to yield an explicit expression for the dimensionless particle length as a function of time,

$$L(\tau)=\frac{1}{\sqrt{1-2\varepsilon^2\tau}}. \tag{36}$$

We now use this to substitute into Eq. (33) to provide an explicit expression for Pe, the time-dependent, non-dimensional particle velocity as,

$$Pe(\tau)=\frac{\varepsilon}{\sqrt{1-2\varepsilon^2\tau}}. \tag{37}$$

We can also use eqs. (35) and (36) to evaluate the rate of expansion of the droplet as,

$$\frac{dL}{d\tau}=\frac{\varepsilon^2}{(1-2\varepsilon^2\tau)^{3/2}}. \tag{38}$$

Finally, Eq. (33) is integrated to provide the position of the migrating particle as a function of dimensionless time, namely,

$$x_p(\tau)=\int_0^\tau Pe(s)ds=\frac{1}{\varepsilon}\left(1-\sqrt{1-2\varepsilon^2\tau}\right), \tag{39}$$

where $x_p=\tilde{x}_p/\tilde{L}_0$ represents the dimensionless position of the particle in the laboratory frame, assuming an initial position of $x_p=0$.

4. Results

4.1. Solution behavior

The approximate solutions for the several quantities involved with TGZM, represented by eqs. (36)–(39), are shown in Fig. 3. The dimensionless particle length and its velocity change over time with the same functional dependence, and both L and $\varepsilon^{-1}Pe$ are plotted as a function of scaled dimensionless time, $\varepsilon^2\tau$, by the solid curve. Note that the particle length and speed initially slowly increase with time, but there is a rapid increase after $\varepsilon^2\tau\approx 0.4$, and both features approach a mathematical limit of infinity as $\varepsilon^2\tau\to 0.5$.

The rate of particle expansion, as expressed by Eq. (38), is plotted as $\varepsilon^{-2}dL/d\tau$ versus scaled dimensionless time, $\varepsilon^2\tau$, by the dashed curve in Fig. 3. While the absolute measure of particle expansion is quite small, as indicated by its prefactor of ε^2, it increases in time much more quickly than the particle length and velocity. As is clear from its mathematical representation, the particle expansion rate also approaches infinity as $\varepsilon^2\tau\to 0.5$.

Finally, the scaled particle position, εx_p, is plotted as a function of scaled dimensionless time, $\varepsilon^2\tau$, by the dotted curve in Fig. 3. Interestingly, this nonlinear curve does not increase as fast as the other measures and remains finite at the value of $\varepsilon^2\tau=0.5$; however, x_p becomes a complex number for values of time exceeding this limit.

Another representation of particle migration is provided by Fig. 4, which shows the behavior of a system with a dimensionless migration parameter of $\varepsilon=0.1$. This plot shows both the dimensionless particle position, x_p, as a function of dimensionless time, τ, and a visualization of the droplet length and concentration and temperature profiles within the droplet at three discrete times during migration. Clearly, the particle position, x_p, increases with time in a nonlinear fashion. In addition, the color depiction of the concentration within the particles shows that the profile is linear, with higher concentration on the left side, where the excess component is rejected at the growth interface, and with lower concentration on the right side, adjacent to dissolving matrix. The excess component diffuses across the droplet in the growth direction, and the average composition decreases with time as the particle lengthens while migrating. The temperature profile across the droplets is also linear, and its average increases with time as the particle migrates up the temperature gradient.

4.2. Solution validity

We have applied a number of assumption to derive our approximate TGZM solution. In the following discussion, we aim to examine the conditions under which these approximations are valid. We also present a listing of relevant physical properties and parameters for several TGZM systems, including Te-rich inclusions in CdTe, brine droplets in ice, and acetone-rich droplets within a succinonitrile alloy (SCN-ACE), in Table 1.

4.2.1. Initial scaling arguments

We first consider the quasi-steady-state (QSS) approximation, whereby all time derivatives are set to zero in the dimensionless equations. This is justified when the time scale for the lengthening of the particle is much less than the diffusion time scale used to nondimensionalize time.

Let us define τ_L as the characteristic time scale for changes in the particle size and rewrite the evolution equation for particle length, Eq. (35), in terms of a dimensionless time, $\tau^*\equiv t/\tau_L$,

$$\frac{\tau_{\mathcal{D}}}{\tau_L}\frac{dL}{d\tau^*}=\varepsilon^2L^3, \tag{40}$$

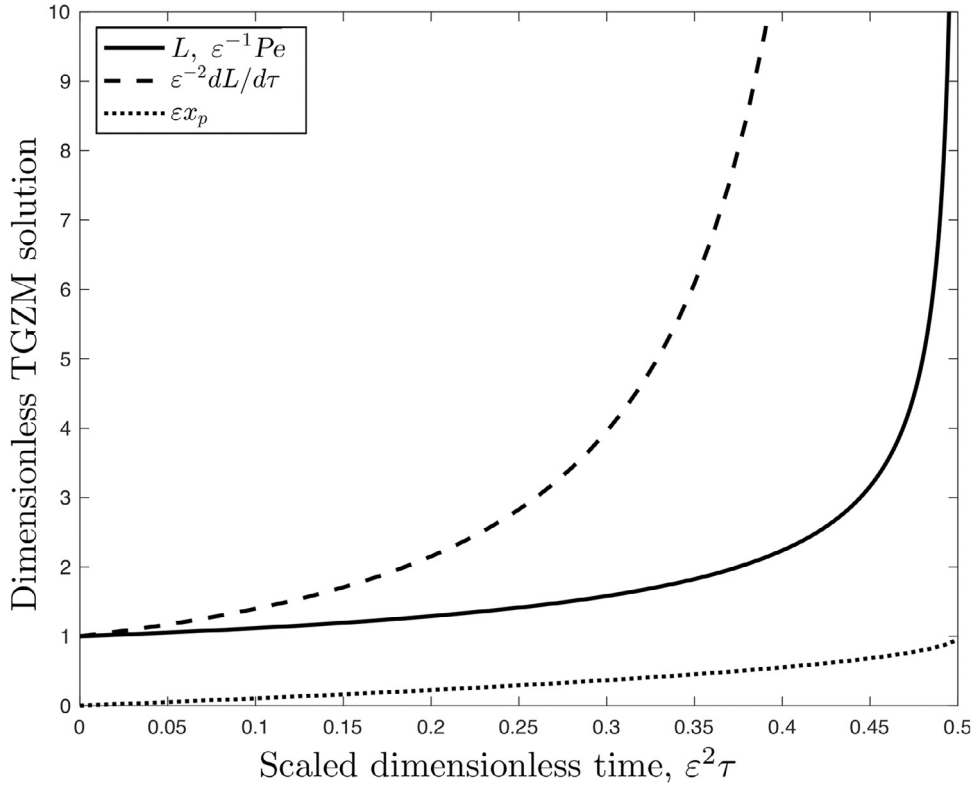

Fig. 3. Measures of the TGZM solution, namely dimensionless particle length, L, scaled dimensionless particle velocity, $\varepsilon^{-1}Pe$, scaled dimensionless particle expansion, $\varepsilon^{-2}dL/d\tau$, and scaled dimensionless particle position, εx_p, are plotted as functions of scaled dimensionless time, $\varepsilon^2\tau$.

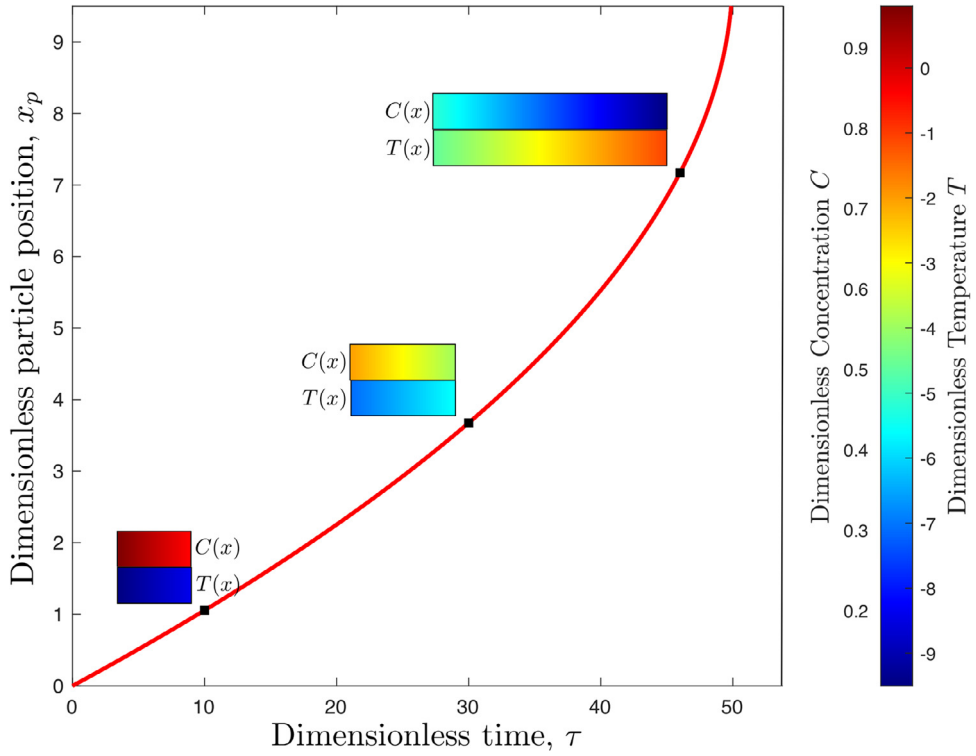

Fig. 4. Dimensionless particle position, x_p, is plotted as a function of dimensionless time, τ, for a system with $\varepsilon = 0.1$. Bars plotted at discrete times represent particle length, with interiors colored by values of dimensionless concentration, $C(x)$, and temperature, $T(x)$, through the particle (color scales are indicated on right). The excess component is rejected at the growth interface (left side) and diffuses across the particle to the dissolution interface (right side). As the particle lengthens, its average concentration decreases and its average temperature increases.

Table 1
Physical properties and parameters of TGZM systems. Representative values are preceded with ∼.

Property/parameter	Units	CdTe-Te [25,50,51]	Brine-ice [47]	SCN-ACE [11,52]
C_p	J/(kg K)	187	4200	2000
$\mathcal{D}$	m^2/s	$\sim 10^{-10}$	$\sim 10^{-10}$	$\sim 10^{-10}$
G	K/m	3500	100	8000
k_s	W/(mK)	0.907	2.811	0.19
k_ℓ	W/(mK)	6	0.54	0.19
$m\tilde{C}_0$	°C	~ 10	~ 10	~ 10
$\tilde{L}_0$	m	$\sim 10^{-5}$	$\sim 10^{-5}$	$\sim 10^{-5}$
V	m/s	$\sim 5.29 \times 10^{-9}$	$\sim 5.21 \times 10^{-9}$	$\sim 8.00 \times 10^{-8}$
α_ℓ	m^2/s	5.65×10^{-6}	1.29×10^{-7}	9.63×10^{-8}
$-\Delta H_f$	J/kg	2.09×10^5	3.34×10^5	3.92×10^5
ρ_ℓ	kg/m^3	5680	1000	987
Dimensionless group	Definition	CdTe-Te	Brine-ice	SCN-ACE
Migration parameter, ε	$\frac{\kappa G\tilde{L}_0}{m\tilde{C}_0}$	5.29×10^{-4}	5.21×10^{-4}	8.00×10^{-3}
Conductivity ratio, κ	$\frac{k_s}{k_\ell}$	0.151	5.21	1.00
Lewis number, Le	$\frac{\alpha_\ell}{\mathcal{D}}$	5.65×10^4	1.29×10^3	9.62×10^2
Peclet number, Pe	$\frac{V\tilde{L}_0}{\mathcal{D}}$	5.29×10^{-4}	5.21×10^{-4}	8.00×10^{-3}
Stefan number, Sf	$\frac{-\Delta H_f}{C_p\kappa G\tilde{L}_0}$	2.11×10^5	1.53×10^4	2.45×10^3
$Pe_h = \mathrm{Le}^{-1}Pe$	$\frac{V\tilde{L}_0}{\alpha_\ell}$	9.37×10^{-9}	4.05×10^{-7}	8.31×10^{-6}
$SfLe^{-1}Pe$	$\frac{-\Delta H_f V}{k_s G}$	1.98×10^{-3}	6.19×10^{-3}	2.04×10^{-2}

where $\tau_\mathcal{D} \equiv \tilde{L}_0^2/\mathcal{D}$ is the diffusion time scale employed in the definition, $\tau \equiv t/\tau_\mathcal{D}$. With this new dimensionless time, we argue that $dL/d\tau^*$ and L are $\mathcal{O}(1)$ quantities. This implies that the leading terms on both sides of this equation can be equated,

$$\frac{\tau_\mathcal{D}}{\tau_L} = \varepsilon^2, \tag{41}$$

where ε is the dimensionless migration parameter defined by Eq. (7). The QSS approach is justified when the diffusion time scale is much smaller than the time scale for particle lengthening. which is true when, using the above ratio of these scales is very small or,

$$\varepsilon^2 \ll 1. \tag{42}$$

This condition is easily met for all systems listed in Table 1 and for nearly all TGZM systems of interest.

Our next assumption, invoked to justify the derivation of the concentration profile through the droplet, defined by Eq. (9), is that the dimensionless Peclet number is very small, $Pe \ll 1$. From Eq. (33), we know that $Pe = \varepsilon L$. Taking $L(0) = 1$, then we require that,

$$Pe \sim \varepsilon \ll 1. \tag{43}$$

This is slightly more restrictive than argued above for the validity of the quasi-steady-state (QSS) assumption, namely if Eq. (43) holds, then it must also be true that $\varepsilon^2 \ll 1$.

Finally, we invoked two simplifications to solve for the temperature field across the particle. First, we argued that both terms on the left-hand-side of Eq. (19), representing accumulation and convection, could be ignored when,

$$Le^{-1}Pe \ll 1. \tag{44}$$

However, $Le \gg 1$ for nearly all liquids, so this requirement is easily satisfied, particularly since we have already specified that $Pe \ll 1$. This "thermal pseudosteady assumption" is commonly employed for the analysis of solidification at small length scales, most notably by Mullins and Sekerka in their classic analysis of constitutional supercooling [31]. Second, we argued that latent heat is negligible in the interfacial heat balance conditions, eqs. (23) and (24), which is true when,

$$SfLe^{-1}Pe \ll 1. \tag{45}$$

This condition is typically satisfied, even if the dimensionless Stefan number, Sf, is relatively large, owing to the validity of the prior requirement, Eq. (44). All of these assertions are consistent with the tabulated values shown in Table 1.

4.2.2. Temporal evolution

The nonlinear temporal evolution of the TGZM solutions gives rise to another set of considerations for solution validity. An obvious limitation is evident in the expressions for particle length and velocity, Eqs. (36) and (37), which are finite only for $\varepsilon^2\tau \le 0.5$. A less apparent physical contradiction occurs when $\varepsilon^2\tau = 0.5 - \varepsilon/4$, when the minimum concentration in the droplet becomes negative.

However, even before these mathematical limits are reached, the nonlinear increase of particle length calls for a re-examination of our scaling requirement that $Pe \ll 1$ in Eq. (10), as discussed in the previous section. If we define a dynamic Peclet number using the time-dependent length, $\tilde{L}(\tau)$, we get

$$Pe^* = \frac{V(\tau)\tilde{L}(\tau)}{\mathcal{D}} = PeL(\tau) \ll 1, \tag{46}$$

where Pe^* is the dynamic Peclet number and Pe is our original definition using initial particle length, $\tilde{L}_0$. Using $Pe = \varepsilon L$ from Eq. (33), we can rewrite this condition as,

$$\varepsilon L^2 \ll 1, \tag{47}$$

or,

$$L \ll \frac{1}{\sqrt{\varepsilon}}. \tag{48}$$

This is more restrictive than the time limits keeping length and velocity to be finite and concentration to be nonzero that were discussed above. For example, using the largest value of the migration parameter of $\varepsilon = 8 \times 10^{-3}$ listed in Table 1, this restriction requires that $L \ll 11$. However, it is increasingly less restrictive for systems with smaller values of the migration parameter. With the value of $\varepsilon = 5 \times 10^{-4}$, which is characteristic of the other two systems listed in Table 1, this limitation becomes $L \ll 45$.

We finish our discussion of solution validity by rearranging the above condition, Eq. (48), to,

$$\varepsilon \ll 1/L^2. \tag{49}$$

Satisfying this requirement guarantees that $\varepsilon \ll 2/L^2$, the condition previously stated by Eq. (29), thereby validating the derivation of the temperature field across the droplet, expressed by Eq. (30), in Section 3.3.

5. Conclusions

We have derived an approximate analytical solution to describe the time-dependent migration of liquid droplets through a solid under a thermal gradient, a physical process also referred to as temperature gradient zone melting or TGZM. In contrast to historical analyses, we provide a straightforward derivation of this solution and explain the conditions needed to validate the approximations used in the solution.

Through this analysis, we find that the most important measure of system behavior is the migration parameter, defined as

$$\varepsilon \equiv \frac{\kappa G \tilde{L}_0}{m\tilde{C}_0}, \tag{50}$$

which must be small for our analysis to be valid, specifically $\varepsilon \ll 1$. This parameter represents the driving force for particle migration. From our analysis, we find that the dimensionless particle velocity is simply the migration parameter multiplied by the dimensionless length of the particle, $Pe = \varepsilon L$, as shown by Eq. (33). Rearranging this in dimensional terms, the particle migration velocity is then given as,

$$V(t) = \varepsilon L \frac{\mathcal{D}}{\tilde{L}_0} = \frac{\kappa G \mathcal{D}}{m\tilde{C}_0\left(\frac{\tilde{L}_0}{\tilde{L}(t)}\right)}, \tag{51}$$

where the final expression on the right-hand-side is written exclusively in dimensional terms.

Significantly, this expression for particle velocity is very nearly the same as Eq. (1), the formula derived in the classical analysis of Tiller [45] and others [8,38,41,47,48]. Indeed, for our idealized material system with $K = 0$, one readily sees that two expressions are identical when the ratio of thermal conductivities is taken as unity, $\kappa = 1$, and the particle concentration in Eq. (1) is taken to be $\tilde{C} = \tilde{C}_0(\tilde{L}_0/\tilde{L}(t))$, which is the average concentration in the particle. What is noteworthy about this average concentration is that it changes continuously with time as the particle migrates in time, a subtle but significant effect that seems not to have been included until the much later analysis of Pan et al. [11,12] and the results we have presented above.

The most important limitations of the TGZM model developed here are associated the assumption of one-dimensional behavior. First, under this assumption, our model unduly emphasizes the resistance to heat flow through the liquid particle. In particular with only one spatial dimension, all heat must flow through the particle of the model, whereas, in three-dimensional reality, heat can also flow around particles. Seidenstiker [48] realized this and argued that a correction be applied to the migration velocity using the axial thermal gradient computed for an isolated sphere embedded within a matrix of different conductivity, a problem originally solved by Maxwell [53]. This modification replaces the thermal conductivity ratio, κ, with a new measure, defined as

$$\kappa^* = \frac{3k_s}{2k_s + k_\ell}. \tag{52}$$

Using κ^* with all of the formulas derived here will provide a more accurate description of an initially spherical droplet migrating through a solid, and this value should be employed to apply our model for the description of experimental TGZM data.

Second, while the long-time evolution of the migrating particle is of great interest, the lengthening droplet will alter its shape from spherical to an extended, more cylindrical form, which will give rise to local differences in curvature of the solid-liquid interface. Thus, as explained earlier in the development of our model, a more realistic representation of the equilibrium melting temperature must include Gibbs-Thomson effects. Significantly, these effects may drive break-up of an extended particle via the Rayleigh instability [54,55]. Such particle break-up has been observed by Yang and co-workers [21–25] during the annealing of CdZnTe under thermal gradients. However, representing these phenomena would require at least a two-dimensional model and likely a numerical solution approach.

In spite of these limitations, we believe that our results provide a solid analytical framework for describing the thermal migration of liquid droplets in solids. With this model, these phenomena can be more completely and quantitatively understood.

Declaration of Competing Interest

The authors declare that they have no known competing financial interests or personal relationships that could have appeared to influence the work reported in this paper.

Acknowledgments

This work was supported in part by U.S. Department of Homeland Security, 2012-DN-077-ARI066-02, the content which does not necessarily reflect the position or policy of the United States Government, and no official endorsement should be inferred. The authors would like to thank Prof. Steven Egarievwe, Dr. Ge Yang, Dr. Ralph B. James, and members of the Radiation Detector and Nonproliferation R&D Group at Brookhaven National Laboratory for providing insight to second-phase particles in CdZnTe and their annealing via TGZM. We would also like to acknowledge Professor David Kohlstedt of the University of Minnesota for bringing our attention to geophysical brine pocket migration phenomena. Finally, we wish to thank an anonymous reviewer, whose insightful comments improved the manuscript.

References

[1] W. Pfann, Temperature gradient zone melting, Journal of Metals 7 (9) (1955). 961–961
[2] W. Pfann, Temperature gradient zone-melting, US Patent 2 (1957) 813. 048 (Nov. 1957)
[3] E.E. Gruber, Calculated size distributions for gas bubble migration and coalescence in solids, J Appl Phys 38 (1) (1967) 243–250.
[4] F.A. Nichols, Kinetics of diffusional motion of pores in solids: a review, J. Nucl. Mater. 30 (1–2) (1969) 143–165.
[5] W. Oldfield, A.J. Markworth, The theory of bubble migration applied to irradiated materials, Materials Science and Engineering 4 (6) (1969) 353–366.
[6] D.R. Olander, Study of Thermal-Gradient-Induced Migration of Brine Inclusions in Salt. Final Report, Tech. Rep. BMI/ONWI-538, California Univ., Berkeley (USA), 1984.
[7] A.W. Rempel, E.D. Waddington, J.S. Wettlaufer, M.G. Worster, Possible displacement of the climate signal in ancient ice by premelting and anomalous diffusion, Nature 411 (6837) (2001) 568–571.
[8] D. Allen, J. Hunt, Melting during solidification, Metall. Trans. A 7A (1976) 767.
[9] H.N. Thi, G. Reinhart, A. Buffet, T. Schenk, N. Mangelinck-Noël, H. Jung, N. Bergeon, B. Billia, J. Härtwig, J. Baruchel, In situ and real-time analysis of TGZM phenomena by synchrotron X-ray radiography, J Cryst Growth 310 (11) (2008) 2906–2914.
[10] M. Rettenmayr, Melting and remelting phenomena, Int. Mater. Rev. 54 (1) (2009) 1–17.
[11] S. Pan, Q. Zhang, M. Zhu, M. Rettenmayr, Liquid droplet migration under static and dynamic conditions: analytical model, phase-field simulation and experiment, Acta Mater 86 (2015) 229–239.
[12] S. Pan, M. Zhu, M. Rettenmayr, Phase-field modeling of liquid droplet migration in a temperature gradient, IOP Conference Series: Materials Science and Engineering 84 (2015) 012073.
[13] R. Schwarz, K. Benz, Thermal field influence on the formation of te inclusions in cdte grown by the travelling heater method, J Cryst Growth 144 (3–4) (1994) 150–156.
[14] P. Rudolph, A. Engel, I. Schentke, A. Grochocki, Distribution and genesis of inclusions in CdTe and (Cd,Zn)Te single crystals grown by the bridgman method and by the travelling heater method, J. Crystal Growth 147 (1995) 297.
[15] T.E. Schlesinger, J.E. Toney, H. Yoon, E.Y. Lee, B.A. Brunett, L. Franks, R.B. James, Cadmium zinc telluride and its use as a nuclear radiation detector material, Materials Science and Engineering: R: Reports 32 (4–5) (2001) 103–189.
[16] G.A. Carini, A.E. Bolotnikov, G.S. Camarda, G.W. Wright, R.B. James, L. Li, Effect of Te precipitates on the performance of CdZnTe detectors, Appl Phys Lett 88 (14) (2006) 143515.

[17] H.R. Vydyanath, Recipe to minimize Te precipitation in CdTe and (Cd,Zn)Te crystals, Journal of Vacuum Science & Technology B: Microelectronics and Nanometer Structures 10 (4) (1992) 1476.
[18] H. Vydyanath, J. Ellsworth, J. Parkinson, J. Kennedy, B. Dean, C. Johnson, G. Neugebauer, J. Sepich, P. Liao, Thermomigration of te precipitates and improvement of (Cd,Zn)Te substrate characteristics for the fabrication of LWIR (hg,cd)te photodiodes, J. Electronic Materials 22 (8) (1993) 1073–1080.
[19] T. Lee, J. Park, Y. Jeoung, H. Kim, C. Chun, J. Kim, L. Park, J. Chang, S. Kim, M. Park, Thermomigration of tellurium precipitates in CdZnTe crystals grown by the vertical bridgman method, J. Electron. Mater. 24 (9) (1995) 1053–1056.
[20] M. Meier, M. Harrison, S. Spalsbury, D. McGregor, Laser-induced thermomigration of Te precipitates in CdZnTe crystals, J. Crystal Growth 311 (2009) 4247–4250.
[21] G. Yang, A.E. Bolotnikov, P.M. Fochuk, G.S. Camarda, Y. Cui, A. Hossain, K. Kim, J. Horace, B. McCall, R. Gul, L. Xu, O.V. Kopach, R.B. James, Study on thermal annealing of cadmium zinc telluride (CZT) crystals, in: A. Burger, L.A. Franks, R.B. James (Eds.), Hard X-Ray, Gamma-Ray, and Neutron Detector Physics XII, Vol. 7805, 2010. 780507–780507–8
[22] G. Yang, A. Bolotnikov, P. Fochuk, Y. Cui, G.S. Camarda, A. Hossain, K.H. Kim, J. Horace, B. McCall, R. Gul, O. Kopach, S. Egarievwe, R. James, Post-growth annealing of cadmium zinc telluride crystals for room-temperature radiation detectors, J. Electron. Mater. 41 (10) (2012) 2912–2916.
[23] A.L. Adams, A. Kassu, W. Chan, M. Drabo, R. Pinder, S. Egarievwe, A. Radja, G. Yang, R.B. James, Thermal annealing: a technique to improve the performance of cadmium zinc telluride (CZT) material for semiconductor radiation detector applications, in: Fluids and Heat Transfer, Parts A, B, C, and D, Vol. 7 of ASME International Mechanical Engineering Congress and Exposition, 2012, pp. 29–33.
[24] K. Kim, J. Suh, A.E. Bolotnikov, P.M. Fochuk, G.S. Kopach, O.V. Camarda, Y. Cui, Y. Cui, A. Hossain, G. Yang, J. Hong, R.B. James, Temperature-gradeint annealing of CdZnTe under te overpressure, J. Crystal Growth 354 (2012) 62–66.
[25] G. Yang, A.E. Bolotnikov, P.M. Fochuk, G.S. Camarda, A. Hossain, U.N. Roy, Y. Cui, R. Pinder, J. Gray, R.B. James, Thermo-migration of Te inclusions in CdZnTe during post-growth annealing in a temperature-gradient field, Physica Status Solidi C 11 (7–8) (2014) 1328–1332.
[26] A. Zappettini, N. Zambelli, G. Benassi, D. Calestani, M. Pavesi, Live-monitoring of te inclusions laser-induced thermo-diffusion and annealing in cdznte crystals, Appl Phys Lett 104 (25) (2014) 252105.
[27] P. Fochuk, Z. Zakharuk, Y. Nykonyuk, A. Rarenko, M. Kolesnik, A.E. Bolotnikov, G. Yang, R.B. James, Advantages of a special post-growth THM program for the reduction of inclusions in CdZnTe crystals, IEEE Trans Nucl Sci 63 (3) (2016) 1839–1843.
[28] W.G. Whitman, Elimination of salt from sea-water ice, American Journal of Science s5-11 (62) (1926) 126–132.
[29] V. Stefansson, The Friendly Arctic: The Story of Five Years in Polar Regions, Macmillan, 1921.
[30] W.A. Tiller, K.A. Jackson, J.W. Rutter, B. Chalmers, The redistribution of solute atoms during the solidification of metals, Acta Metall. 1 (1953) 428.
[31] W.W. Mullins, R.F. Sekerka, Stability of a planar interface during solidification of a dilute binary alloy, J. Appl. Phys. 35 (1964) 444–451.
[32] Z. Bi, R. Sekerka, Phase field modeling of shallow cells during directional solidification of a binary alloy, J. Crystal Growth 237–239 (2002) 138–143.
[33] E. Meca, M. Plapp, Phase-field study of the cellular bifurcation in dilute binary alloys, Metallurgical and Materials Transactions A 38 (7) (2007) 1407–1416.
[34] Y. Ma, M. Plapp, Phase-field simulations and geometrical characterization of cellular solidification fronts, J. Crystal Growth 385 (2014) 140–147.
[35] J. Wernick, Effects of crystal orientation, temperature, and molten zone thickness in temperature-gradient zone-melting, J. Metals 8 (209) (1957) 1169–1173.
[36] A.I. Mlavsky, M. Weinstein, Crystal growth of gaas from ga by a traveling solvent method, J Appl Phys 34 (9) (1963) 2885.
[37] W. Kingery, W. Goodnow, Brine migration in salt ice, ice and snow: properties, Processes, and Applications (1963) 237–247.
[38] W. Wilcox, Removing inclusions from crystals by gradient trechniques, Ind Eng Chem 60 (3) (1968) 13–23.
[39] T.R. Anthony, H.E. Cline, Thermal migration of liquid droplets through solids, J Appl Phys 42 (9) (1971) 3380–3387.
[40] H.E. Cline, T.R. Anthony, The thermomigration of liquid droplets through grain boundaries in solids, Acta Metall. 19 (6) (1971) 491–495.
[41] H.E. Cline, T.R. Anthony, Effects of the magnitude and crystallographic direction of a thermal gradient on droplet migration in solids, J Appl Phys 43 (1) (1972) 10–15.
[42] D.R.H. Jones, The determination of the kinetics of ice-brine interfaces from data on temperature-gradient zone migration, Philos. Mag. 25 (1) (1972) 97–103.
[43] D.R.H. Jones, The temperature-gradient migration of liquid droplets through ice, J Cryst Growth 20 (2) (1973) 145–151.
[44] D. Jones, Determination of the kinetics of ice-brine interfaces from the shapes of migrating droplets, J Cryst Growth 26 (1) (1974) 177–179.
[45] W.A. Tiller, Migration of a liquid zone through a solid: Part I, J Appl Phys 34 (9) (1963) 2757.
[46] D.T.J. Hurle, J.B. Mullin, E.R. Pike, The motion of liquid alloy zones along a bar under the influence of an electric current, The Philosophical Magazine: A Journal of Theoretical Experimental and Applied Physics 9 (99) (1964) 423–434.
[47] P. Hoekstra, T.E. Osterkamp, W.F. Weeks, The migration of liquid inclusions in single ice crystals, Journal of Geophysical Research (1896–1977) 70 (20) (1965) 5035–5041.
[48] R.G. Seidensticker, Comment on Paper by P. Hoekstra, in: T. Osterkamp, W.F. Weeks (Eds.), 'The migration of liquid inclusions in single ice crystals', volume 71, Journal of Geophysical Research, 1966, pp. 2180–2181.
[49] R.L. Shreve, Migration of air bubbles, vapor figures, and brine pockets in ice under a temperature gradient, J. Geophys. Res. 72 (16) (1967) 4093–4100.
[50] S. Kuppurao, S. Brandon, J.J. Derby, Modeling the vertical bridgman growth of cadmium zinc telluride i. quasi-steady analysis of heat transfer and convection, J Cryst Growth 155 (1) (1995) 93–102.
[51] S. Zhu, C. Li, C.-H. Su, B. Lin, H. Ban, R. Scripa, S. Lehoczky, Thermal diffusivity, thermal conductivity, and specific heat capacity measurements of molten tellurium, J Cryst Growth 250 (1) (2003) 269–273.
[52] D. i. for physical properties sponsored by AIChesuccinonitrile, DIPPR Project 801 - Full version, Design Institute for Physical Property Research/AIChE, 2005. 1–1
[53] J.C. Maxwell, Treatise on Electricity and Magnetism, 1st Edition, Clarendon Press, Oxford, 1873.
[54] L. Rayleigh, On the instabilities of jets, Proc. Lond. Math. Soc. 10 (1878) 4–13.
[55] H. Wong, M.J. Miksis, P. Voorhees, S.H. Davis, Universal pinch off of rods by capillarity-driven surface diffusion, Scr Mater 39 (1) (1998) 55–60.